Available online at www.sciencedirect.com
ScienceDirect
Journal of Nuclear Materials 356 (2006) 168–177
journal of nuclear materials
www.elsevier.com/locate/jnucmat

Effects of pitting damage on fatigue limit and lifetime in mercury target

M. Futakawa *, T. Naoe, H. Kogawa, M. Teshigawara, Y. Ikeda

Quantum Beam Science Directorate, Japan Atomic Energy Agency, Tokai-mura, Ibaraki-ken, Naka-gun 319-1195, Japan

Abstract

High power spallation targets for neutron source are being developed in the world. Mercury target will be installed at the material and life science facility in J-PARC, which will promote innovative science. The moment the proton beams bombard the mercury target, pressure waves will be generated in mercury by thermally shocked heat deposition. Cavitation will be induced through the pressure wave propagation in the mercury and erode the vessel inner surface contacting with mercury, i.e. pitting damage. The eroded vessel wall is damaged by cyclic fatigue because pulsed proton beams strike the target repeatedly. It is, therefore, important to evaluate the fatigue strength of the eroded vessel wall from the viewpoint of target lifetime estimation. In the paper, we describe the effects of pitting damage, cyclic fatigue damage and mercury environment on the lifetime of the mercury target.

1. Introduction

A liquid-mercury target system for the MW-class target is being developed in the JAEA as taking into account the neutron yield and self-circulating heat removal efficiencies, and will be installed at the material and life science facility in J-PARC (Japan Proton Accelerator Research Complex) [1]. The proton beam with a 1 μs pulse duration is injected into the mercury through a beam window at 25 Hz. The moment the proton beams bombard the target, stress waves will be imposed on the beam window and pressure waves will be generated in the mercury by thermally shocked heat deposition [2,3]. Provided that the negative pressure generates through the pressure wave propagation in the mercury target, there is a possibility for the formation of cavitation in mercury and the cavitation of micro-bubbles collapses to form pits on the interface between mercury and the target vessel under proton injection [4]. Off-line tests on the pressure waves without proton beam had been carried out to evaluate the dynamic response of mercury by using an SHPB (Split Hopkinson Pressure Bar) impact machine. We found the pitting damage on the interface between solid metals and mercury [5,6]. Following SHPB tests, on-beam tests using proton beam had been performed to confirm the pitting damage observed in the off-line tests [7]. After both the experimental results, the so-called pitting damage becomes as a crucial issue to the

* Corresponding author. Tel.: +81 29 282 5363; fax: +81 29 282 6712.
E-mail address: futakawa.masatoshi@jaea.go.jp (M. Futakawa).

0022-3115/$ - see front matter © 2006 Elsevier B.V. All rights reserved.
doi:10.1016/j.jnucmat.2006.05.018

lifetime of the target vessel and the realization of high power spallation neutron sources.

In order to systematically examine the pitting damage formation on the target vessel under certain conditions, off-line tests were performed using an innovative device, MIMTM (electroMagnetic IMpact Testing Machine) to simulate the pressure waves due to proton bombarding mercury [8]. From the viewpoint of the lifetime estimation, we have to consider cyclic fatigue damage on the pitting-damaged vessel wall, because the target vessel is subjected to impulsive pressures at 25 Hz repeatedly. Actually, the pitting and fatigue damages will be imposed on the vessel wall at the same time. To precisely investigate the effects of the damages, the pitting damage was evaluated against the number of pulses, and then the fatigue test was carried out using the pitting-damaged specimens. In this paper, the effects of the pitting damage, cyclic fatigue and mercury environment on the lifetime estimation will be discussed based on the data obtained by the off-line tests.

2. Experiment

Fig. 1 shows the mercury chamber and specimen in the MIMTM that can impose the impulsive pressure equivalent to that induced by MW-class proton beam bombarding on the interface between mercury and target vessel wall. The impulsive pressure is imposed to the mercury through the disk plate driven with the striker controlled by the electric power to electromagnetic coils in the MIMTM. The magnitude of pressure is varied by the imposed power into the MIMTM. The morphology of pitting damage observed at electric power of 560 W in the MIMTM was sufficiently similar to that obtained by the on-beam tests at Weapons Neutron Research

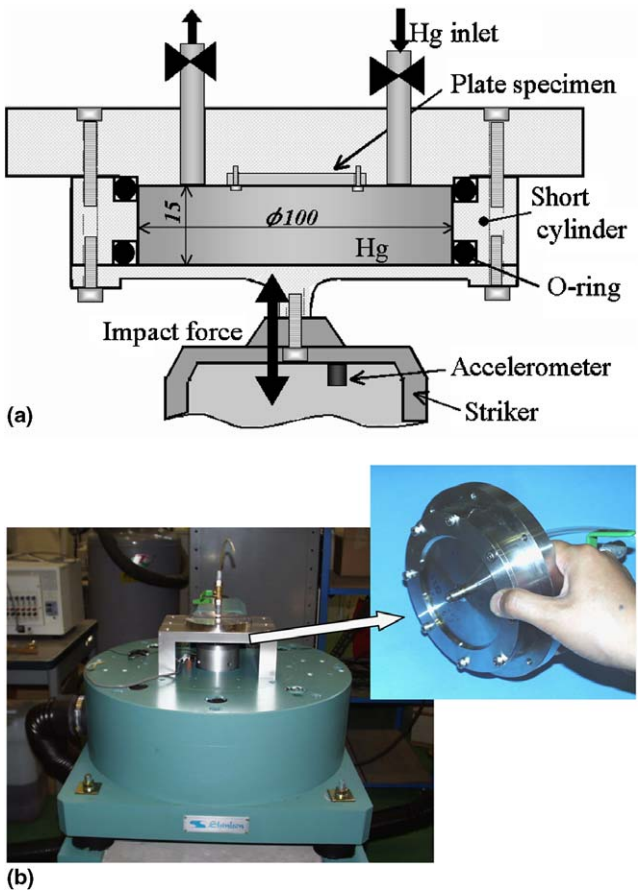

Fig. 1. (a) Schematic drawing of Hg chamber with striker driven by electromagnetic force. (b) The MIMTM device to simulate pitting damage on the vessel inner wall in mercury target.

Table 1
Main mechanical properties in SA316SS and CW316KL

	Young's modulus, GPa	Y.S. (0.2%), MPa	T.S., MPa	K_J,[a] MPa$\sqrt{m}$
SA316SS	190	249	525	393
CW316KL	193	725	785	85

[a] Pawel et al. [9].

facility (WNR) in Lao Alamos National Laboratory, assuming MW-class proton beams [7,8]. In the MIMTM test, the frequency of pulses is 25 Hz, which is the same as that in J-PARC.

The materials of specimen are annealed austenitic stainless steel AISI 316, (SA316SS) and 20% cold worked AISI 316 with carburizing surface improvement, Kolsterising® (CW316KL). The main mechanical properties are shown in Table 1. The plate specimen, $60 \times 60 \times 2.5\ mm^3$, is set in the mercury chamber, as illustrated in Fig. 1. The thickness is equal to that of the JSNS target beam window which will be most likely suffered with pitting damage. The morphology and depth profile of pits are observed using a SEM and a laser microscope.

Three-point bending fatigue tests were carried out using the specimen, $4.0 \times 60 \times 2.5\ mm^3$, cut from the plate specimen with pitting damage that was imposed to various numbers of pulses at 560 W. An electromagnet-force fatigue machine with a frequency range from 1 Hz to 1 kHz and the maximum load 1 kN was used for high cycle fatigue tests. In the test, the repeated frequency is 100 Hz and loading ratio R is 0.1. In the three-point bending, the distance between supporting the two points is 30 mm and the bending load is applied at the center of specimen.

The fatigue tests were carried out in load-controlled condition under mercury in atmosphere at room temperature to evaluate the effect of mercury on the fatigue strength. The displacement and load were measured at the center of specimens by a laser displacement gage (Keyence LK-035) and load cell (Kyowa LUK-A-5KNSA1), respectively.

3. Results

3.1. Pitting damage

Fig. 2 shows the micrographs and 3D-images of pitting damage on the SA316SS specimens taken with a laser microscope. The pitting damage is strongly dependent on the number of cycles. The

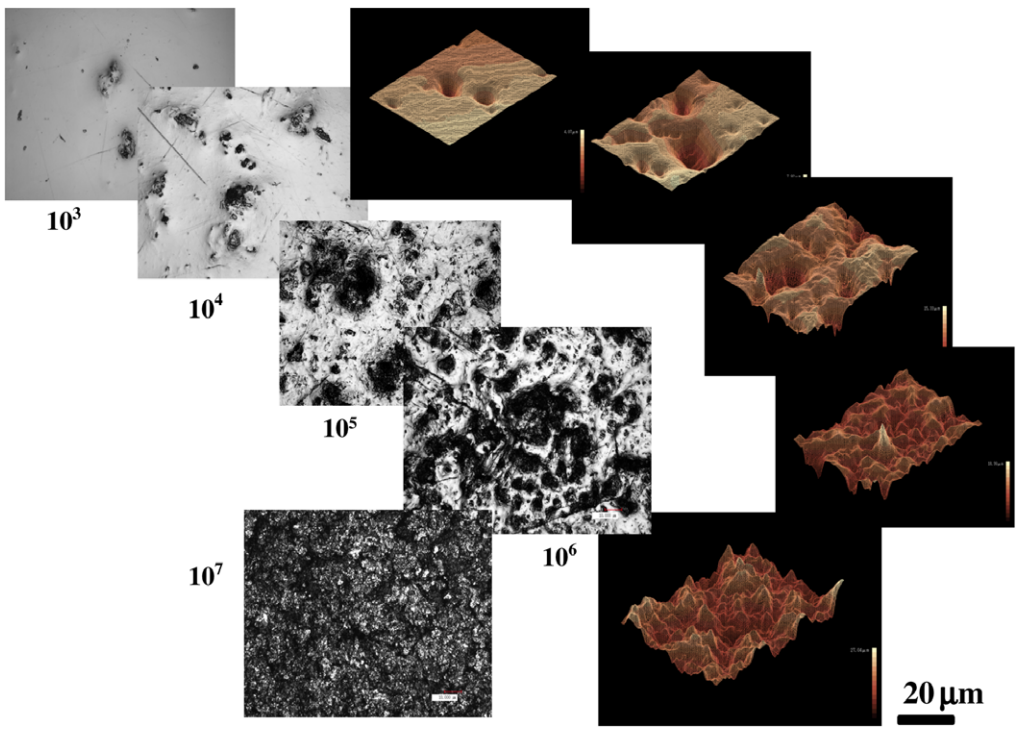

Fig. 2. Micrographs and 3D-images of pitting damage on SA316SS specimens.

pits of 30 μm in diameter are readily observed in the case of the surface imposed to 10^3 impacts. On many locations, the specimen surface is slightly damaged with formation of shallow dishes or craters. The typical pit depth is about 4 μm. The pitting damage around 10^4 cycles looks to be occupied by individual isolated pits. A quite similar morphology of pits was observed in the SHPB [6] and the WNR test [7]. As the number of cycles increases to more than 10^5, the individual isolated pits appear to be combined each other or overlapped and the surface around pits is eroded by peeling out. The pits spread widely over the specimen surfaces after being subjected to over 10^5 impacts. Many pits overlap and form a line patch or round patch. The typical pit depth reaches about 6 μm. Since many pits overlap and combine together, it is difficult to identify an area free from pitting damage. Only a few narrow web lines could be the original surface. In addition, the surface profile reveals the presence of cliff-like pits. At the stage after the pitting damage on the specimen surfaces being subjected to 10 million impact cycles, the original surface layer is severely eroded away with many large pits overlapped. Many cracking lines appear among pit groups. The surface erosion with severe pitting damage presents on this specimen. The pit depth should be larger than 14 μm as measured.

From above observations, it is confirmed that the depth and roughness of pits increase with the number of cycles and that the pitting damage formation up to 10 million cycles can be divided into three phases: Phase 1, individual isolated pits are formed up to 10^4 cycles; Phase 2, pits are combined and overlapped and fraction of eroded area becomes nearly equal to 1 between 10^5 and 10^6 cycles; and Phase 3, homogeneous erosion with mass loss starts between 10^6 and 10^7 cycles.

Fig. 3 shows cross-section of the specimens with pitting damage at 10^5, 10^7 and 1.5×10^8 cycles. In particular, the cross-section with pitting damage at 10^7 was chemically etched to recognize the cracks formed under pits. The cracks with length of ca. 10 μm are present. Fig. 4 shows the relationship between the number of pulses and the peak to peak (P–P) roughness measured in the laser microscope. The tendency of the P–P roughness to the number of pulses is divided into three stages: in stage I, the roughness increases by the microplastic deformation due to plural cavitation-bubble microimpacts; in stage II, the homogeneous erosion with mass loss occurs; in stage III, the erosion due to pitting damage is localized and mass loss get to be prominent. The erosion damage is smaller in CW316KL than in SA316SS, as the microplastic deformation is suppressed by the hardened surface in CW316KL.

3.2. Fatigue strength

Fig. 5 shows an example of measured displacement and load as a function of the number of pulses in a three-point bending fatigue test. The imposed load is controlled to be constant at a certain value throughout the tests. The failure was defined as the displacement over 4 mm (the equivalent strain is ca. 0.1). Fig. 6 shows the fatigue endurance curves of SA316SS and CW316KL. The specimens are subjected to the pitting damage with various P–P roughness. Regardless of the materials and the pitting damage, the fatigue strength limit is admitted in the range of over 10^6 cycles, such as conventional fatigue curves of 316SS. For SA316SS, the fatigue curve is hardly affected by the pitting damage with less than 10 μm P–P roughness, i.e. in the stage I as shown in Fig. 4. The pitting damage with the roughness more than 10 μm given in the stages II and III degrades the fatigue strength in the region of the low number of cycles and the fatigue limit which decreases with the increase of the P–P roughness. In particular, the fatigue limit with the P–P roughness of more than 100 μm reduced to about 1/2 times as much as that without any pitting damage. The fatigue strength limit of CW316KL without any pitting damage is ca. 1200 MPa that is much higher than that of SA316SS, ca. 500 MPa, which are evaluated as the maximum stresses at surface using imposed the bending loads. In general the fatigue strength is improved by a cold working treatment. However, even in CW316KL the fatigue degradation due to pitting damage cannot be ignored and gets to be prominent in the stages II and III illustrated in Fig. 4, i.e. the P–P roughness is more than 10 μm. Fig. 7 shows the micrograph of the fracture surface in SA316SS: the number of cycles is 10^5 in fatigue test and the number of pulses 2×10^7 in the MIMTM test. It is confirmed that the P–P roughness of the undulated surface by pits reaches to ca. 30 μm at least and the crack with ca. 20 μm length is present under the pit bottom, which is created by pitting formation as shown in Fig. 3. Typical striation cracking patterns that are normally observed in fatigue fracture surface are distinctly observed around the crack. It is

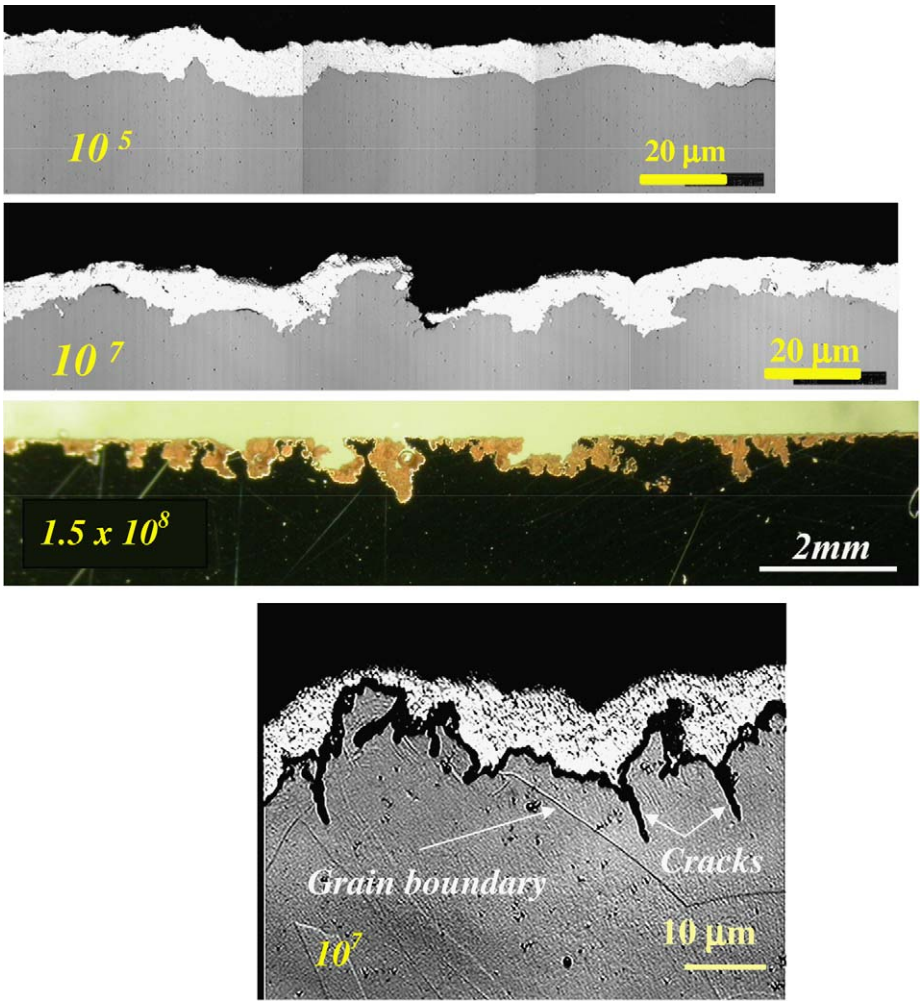

Fig. 3. Cross-sections of the specimens with pitting damage.

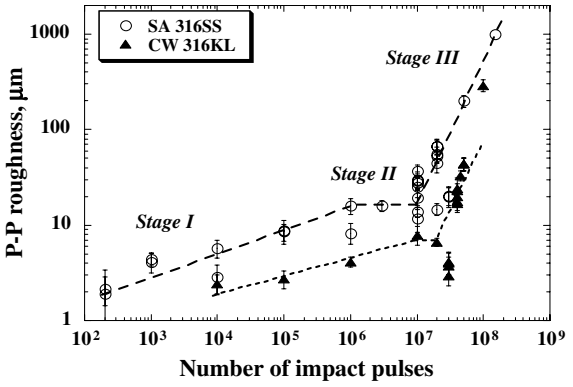

Fig. 4. Relationship between the number of pulses and the peak-to-peak (P–P) roughness. The tendency is divided into three stages: in stage I, the roughness increases with the microplastic deformation; in stage II, the homogeneous erosion with mass loss occurs; in stage III, the erosion due to pitting damage is localized and mass loss gets to be prominent.

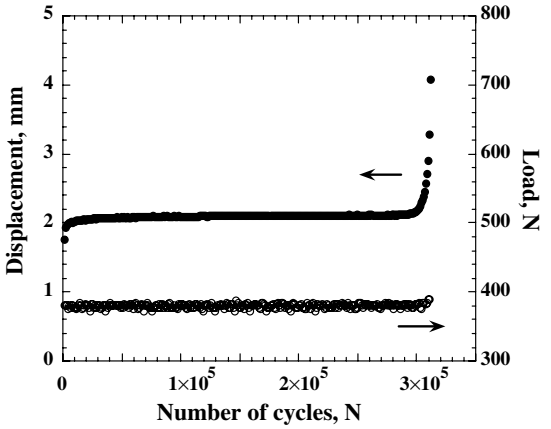

Fig. 5. An example showing measured displacement and load as a function of the number of cycles in the three-point bending fatigue test for SA316SS.

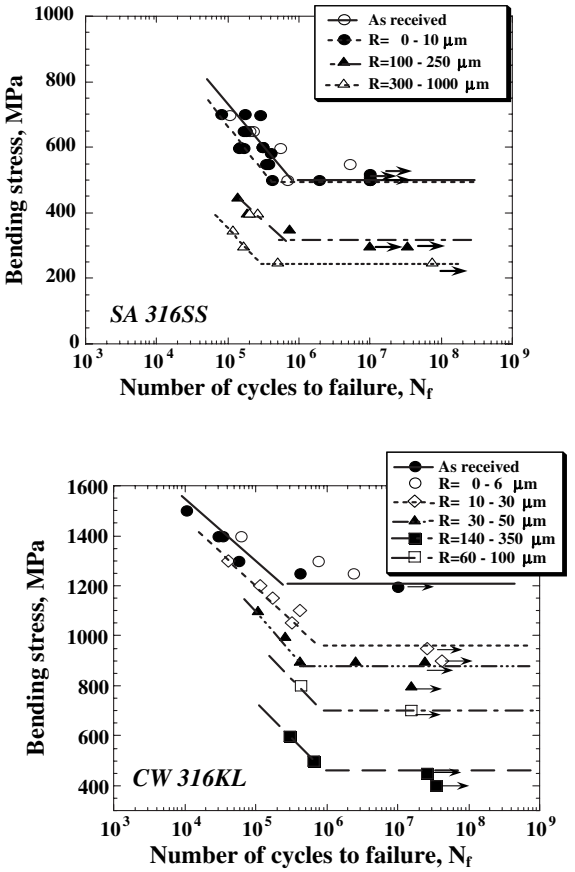

Fig. 6. Fatigue endurance curves of SA316SS and CW316KL at different P–P roughness (R).

believed that the fatigue crack propagation is initiated from the crack formed under the pits.

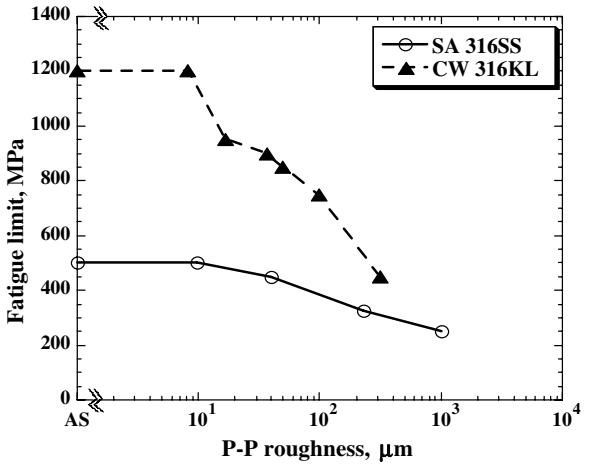

Fig. 8. Relationship between fatigue limit and P–P roughness in SA316SS and CW316KL.

Fig. 8 shows the relationship between fatigue limit and P–P roughness in SA316SS and CW316KL. It is clear that the fatigue limits are not affected by the pitting damage in the range of less than 10 μm P–P roughness, regardless of the materials: SA316SS or CW316KL, and that the roughness sensitivity to the fatigue limit is larger in CW316KL than in SA316SS.

Fig. 9 shows the effect of mercury immersion on fatigue behavior, load–displacement, in CW316SS. In order to specify the fracture surface we used the Vickers indent with 0.5 kN instead of the pits. The number of cycles in mercury immersion is much less than in air, and the displacement increasing-rate close to the fracture is larger in mercury than in

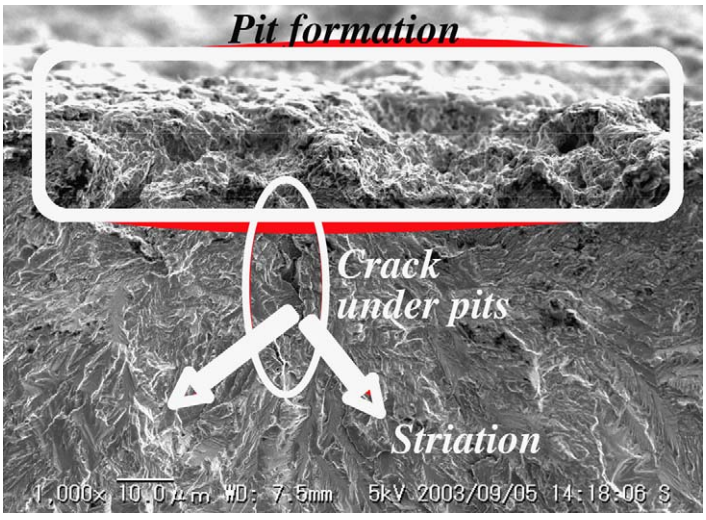

Fig. 7. Micrograph of the fracture surface in SA316SS.

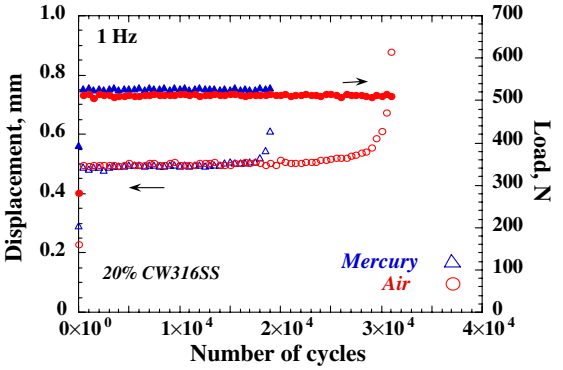

Fig. 9. Effect of mercury immersion on the lifetime of 20% CW316SS in the fatigue tests.

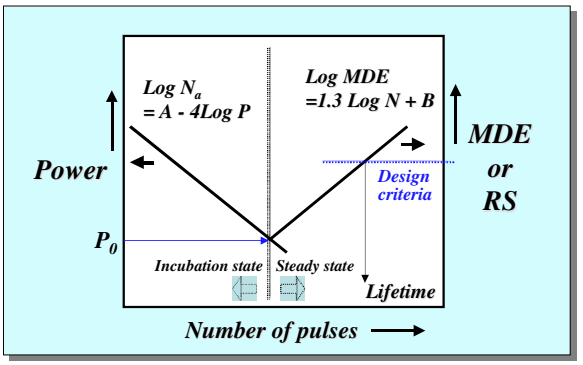

Fig. 11. Conceptual diagram to evaluate the lifetime of mercury target vessel: in the incubation state, the acceptable number of pulses is estimated by $\mathrm{Log}\,N_a = A - 4\log P$ for 316SS, which is predictable with the damage potential evaluated by acoustic vibration. In the steady state, MDE associated with the mass loss is estimated by $\mathrm{Log\,MDE} = 1.3\,\mathrm{Log}\,N + B$ [8,9]. The mass loss is related with the residual strength that is an important value to be compared with the design criteria and to decide the lifetime.

air. The fracture surfaces in mercury immersion and air are shown in Fig. 10. The fracture surfaces are clearly distinguished between them: i.e. the intergranular cracking is dominant on the fracture surface in mercury immersion, while the transgranular cracking is mainly observed in air. The same tendency was reported by Strizak et al. [13].

4. Discussion

Fig. 11 shows a conceptual diagram to estimate the lifetime of the mercury target from the viewpoint of pitting damage [9]. The allowable number of pulses in the incubation period in which the mass loss is hardly induced by the pitting damage is reduced with the increase of power. After the number of pulses becomes larger than the allowable number within the incubation period, the mass loss increases and the residual strength is affected by the pitting damage. As assuming that the residual strength is dominated with the fatigue strength, the fatigue limit (i.e. fatigue strength after 10^6 cycles) is a crucial factor to determine the lifetime of mercury target, because proton pulses will be injected to the target at 25 Hz in JSNS (Japan Spallation Neuron Source) and at 60 Hz at SNS (Spallation Neutron Source). Now, in order to estimate the fatigue limit degradation by the pitting damage we will quantitatively evaluate relationships between the P–P roughness, the number of pressure pulses and the fatigue strength limit.

4.1. P–P roughness and number of pressure pulses

Fig. 12 shows the relationship between the number of pressure pulses and the P–P roughness and the mean depth of erosion (MDE) that is evaluated from the mass loss due to erosion [8]. Futakawa

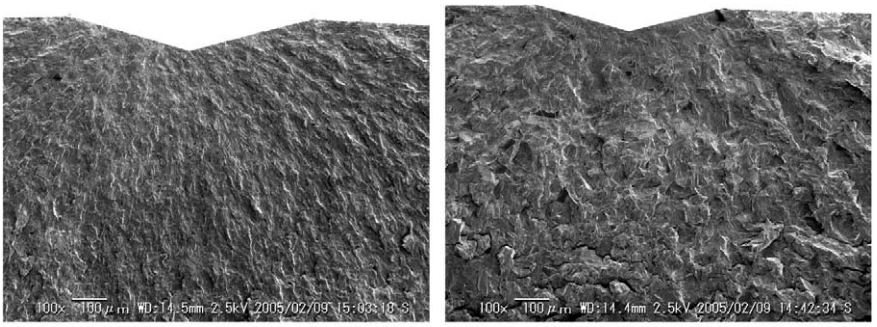

Fig. 10. Micrographs of fracture surface of CW316SS with an indent: (a) in air, (b) in mercury.

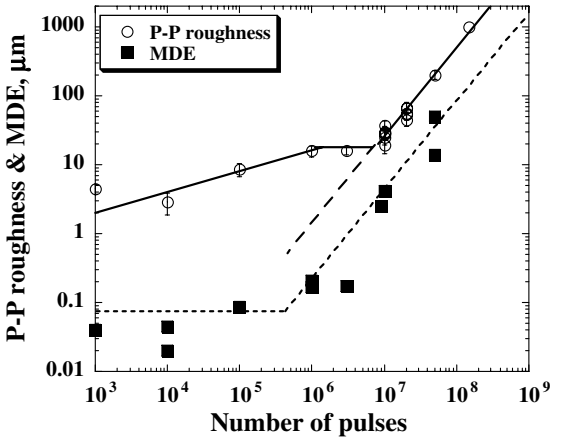

Fig. 12. Relationship between the number of pressure pulses and the P–P roughness and the mean depth of erosion, MDE that was evaluated from mass loss due to erosion.

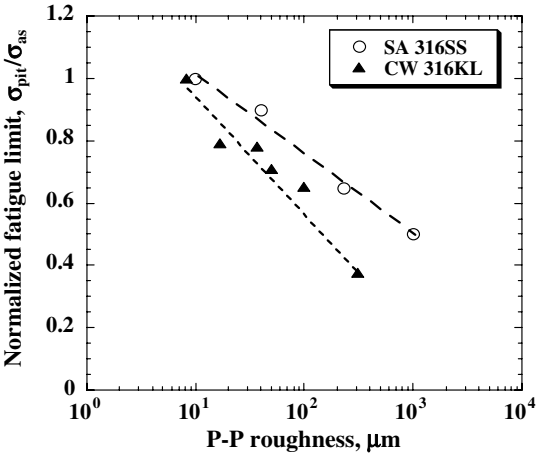

Fig. 13. Relationship between normalized fatigue limit σ_p/σ_{as} (σ_p is the fatigue limit with pitting damage and σ_{as} without any pits) and P–P roughness. The thickness of specimens is 2.5 mm that is equal to the JSNS target beam window suffering from the pitting damage.

et al. [8,10,11] found that the tendency of the MDE to the number of pulses is divided into two states: incubation and steady growth states. In steady growth state the MDE is given by the following equation:

$$\mathrm{Log}\,\mathrm{MDE} = C_1\,\mathrm{Log}N + C_2, \tag{1}$$

where N is the number of pulses and $C_{1,2}$ are material constants. C_1 has been confirmed to be 1.3 regardless of materials [8,11], and C_2 is dependent on the imposed power. It is understandable from Fig. 4 that the inclination of the P–P roughness to the number of pulses in the stage III is almost the same as that in the MDE in this experimental range. It is, therefore, assumed that the P–P roughness, R, is given by

$$\mathrm{Log}R = C_1\,\mathrm{Log}N + C_3, \tag{2}$$

where C_3 is a material constant.

4.2. P–P roughness and fatigue strength limit

Fig. 8 is re-plotted as a semi-log graph using the normalized fatigue strength limit σ_p/σ_{as} (σ_p is the fatigue limit with pitting damage and σ_{as} without any pits.) in Fig. 13. Hence, we recognize that the degradation of fatigue limit due to pitting damage is predictable by using the following equation:

$$\sigma_p/\sigma_{as} = C_4\,\mathrm{Log}R + C_5, \tag{3}$$

where C_4 and C_5 are constants including material and shape factors. It is readily found from Fig. 13 that the fatigue limit of CW316KL is degraded more sensitively by the pitting damage than that of SA316SS since C_4 is −0.26 for SA316SS and −0.37 for CW316KL (in the case of 2.5 mm thickness equal to the beam window in the JSNS target).

4.3. Fatigue limit and number of pulses

The number of pulses in the incubation period, N_{in} is given by

$$\mathrm{Log}N_{in} = C_6\,\mathrm{Log}P + C_7, \tag{4}$$

where P is imposed power and C_6 and C_7 are material constants. C_6 is ca. −4 for 316ss. Hence, using Eqs. (2) and (3), the degradation of fatigue limit σ_p/σ_{as} is described by the following empirical equations:

$$N < N_{in}, \quad \sigma_p/\sigma_{as} = 1, \tag{5}$$

$$N \geqq N_{in}, \quad \sigma_p/\sigma_{as} = C_4(C_1\,\mathrm{Log}N + C_3) + C_5. \tag{6}$$

It had been found that the constants C_1 is 1.3 and C_3 depends on the imposed power [8,10,11]. As a result, the relationship between the degradation of fatigue limit and the number of pulses is illustrated in Fig. 14. The incubation period, i.e. the period at $\sigma_p/\sigma_{as} = 1$, increases with the decrease of power. Since the power density at 560 W in MIMTM seems to be equivalent to the power density of 1 MW in SNS or 0.6 MW in JSNS [12], it is derived from Fig. 11 that the fatigue limit at 10^8

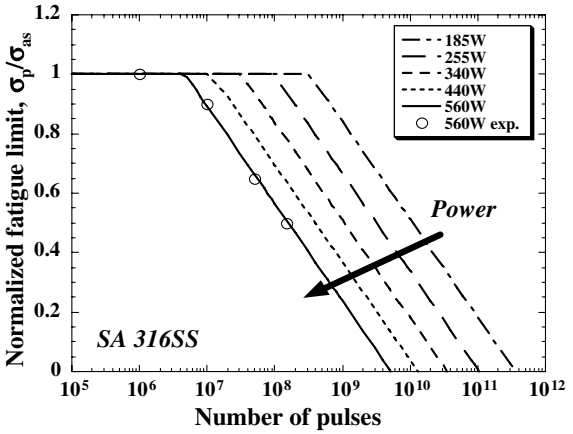

Fig. 14. Relationship between the degradation of fatigue limit and the number of pulses.

pulses decreases to less than $0.5\sigma_{as}$ by the pitting damage in the MW-class mercury target.

Fig. 15 shows the fatigue limit of SA316 and CW316KL as a function of the number of pulses at 560 W of MIMTM. The incubation period of CW316KL is longer than that of SA316SS, while degradation rate due to pitting damage in steady state is higher in CW316KL than in SA316SS. Fatigue crack propagation is influenced by the fracture toughness rather than the material strength. The material strength is effective on the resistance to deformation, i.e. the pitting formation by microplastic deformation. The fracture toughness of CW316KL is lower than that of SA316SS, while the strength of CW316 is higher than that of SA316SS, as shown in Table 1. In order to quantitatively investigate the reason that the degradation rate of fatigue limit of CW316KL is higher than that of SA316SS, we will examine the relationship among the length of cracks formed by pitting, fatigue limit, fracture toughness and stress intensity factor.

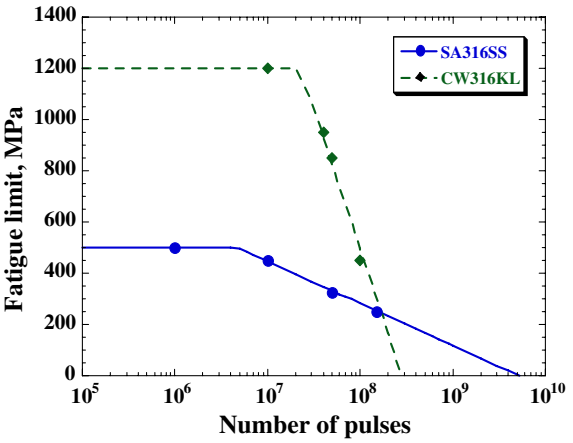

Fig. 15. Fatigue limit of SA316SS and CW316KL as a function of the number of pulses at 560 W in MIMTM. The incubation period of CW316KL is longer than that of SA316SS, while degradation rate due to pitting damage in steady state is higher in CW316KL than in SA316SS.

5. Conclusions

The effect of pitting damage on the fatigue limit was investigated to estimate the lifetime of a mercury target. The empirical equation to estimate the degradation of fatigue limit was derived as taking the pitting damage formation consisting of the incubation and steady states into account. As results, the followings are obtained:

(1) In the results of SA316SS, the pitting damage formation at impact cycles up to 10 million is divided into three phases: Phase 1, isolate individual pits are formed up to 10^4 cycles; Phase 2, pits are combined and overlapped and fraction of eroded area approaches 1 between 10^5 and 10^6 cycles, and; Phase 3, homogeneous erosion with mass loss starts between 10^6 and 10^7 cycles.

(2) The effect of pitting damage on the fatigue limit is categorized into two stages: in the incubation period, the fatigue limit is hardly affected by the pitting; in the steady state, the pitting damage degrades the fatigue limit. That is, the fatigue limit after 10^8 pulses at 0.6 MW in JSNS (1 MW in SNS) decreases to about half of the value without any pitting damage.

(3) The incubation period of CW316KL is longer than that of SA316SS, while degradation rate due to pitting damage in steady state is higher in CW316KL than in SA316SS.

(4) The fatigue strength of CW316 is affected by mercury immersion; the effect of LME on the fatigue is present.

Acknowledgements

The authors would like to thank Emeritus Professor N. Watanabe of JAEA for his fruitful advice and encouragement to this research work, Dr J.R. Haines and Mr B.W. Riemer of ORNL for supplying specimens, and Messrs T. Koyama and T. Ohi of students in Ibaraki University for experiments.

References

[1] Planning Division for Neutron Science, in: Proceeding of the 3rd Workshop on Neutron Science Project – Science and Technology in the 21st Century Opened by Intense Spallation Neutron Source – JAERI-Conf 99-003, 1999.
[2] K. Skala, G.S. Baurer, ICANS XIII, 559–576, 1995.
[3] M. Futakawa, K. Kikuchi, H. Conrad, H. Stechemesser, Nucl. Inst. and Meth. A 439 (2000) 1.
[4] J.M. Carpenter, IWTTHHLM, Schruns, Austria, 1996.
[5] M. Futakawa, H. Kogawa, R. Hino, J. Phys. IV France 10 (2000) 237, Pr9.
[6] M. Futakawa, K. Kogawa, R. Hino, H. Date, H. Takeishi, Int. J. Imp. Eng. 28 (2003) 123.
[7] J.R. Haines, K. Farrell, J.D., Hunn, D.C. Lousteau, L.K. Mansur, T.J. McManamy, S.J. Pawel, B.W. Riemer, Summary of mercury target pitting issue, SNS-101060100-TR0004, 2002.
[8] M. Futakawa, T. Naoe, H. Kogawa, C. Tsai, Y. Ikeda, J. Nucl. Sci. Tech. 40 (2003) 895.
[9] J.E. Pawel et al., J. Nucl. Mater. 212–215 (1994) 442.
[10] M. Futakawa, T. Naoe, C.C. Tsai, H. Kogawa, S. Ishikura, Y. Ikeda, H. Soyama, H. Date, in: 5th Int. Symp. on Cavitation, GS-11-006, Osaka, Japan, November 2003.
[11] H. Soyama, M. Futakawa, Tribol. Lett. 17 (2004) 27.
[12] N. Watanabe, private communication.
[13] J.P. Strizak, H. Tian, P.K. Liaw, L.K. Mansur, Fatigue properties of type 316LN stainless steel in air and mercury, SNS-101060200-TD0001-R00, 2003.